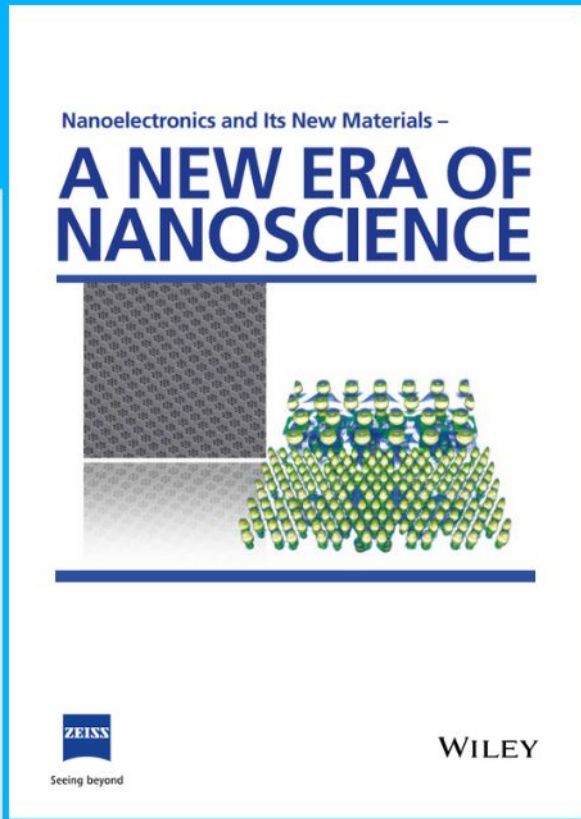




# Nanoelectronics and Its New Materials – A NEW ERA OF NANOSCIENCE



**Discover the recent advances in electronics research and fundamental nanoscience.**

Nanotechnology has become the driving force behind breakthroughs in engineering, materials science, physics, chemistry, and biological sciences. In this compendium, we delve into a wide range of novel applications that highlight recent advances in electronics research and fundamental nanoscience. From surface analysis and defect detection to tailored optical functionality and transparent nanowire electrodes, this eBook covers key topics that will revolutionize the future of electronics.

To get your hands on this valuable resource and unleash the power of nanotechnology, simply download the eBook now. Stay ahead of the curve and embrace the future of electronics with nanoscience as your guide.



Seeing beyond

**WILEY**

# Nano- and Microscale Confinements in DNA-Scaffolded Enzyme Cascade Reactions

Sandra Kröll, Teresa Burgahn, Kersten S. Rabe, Matthias Franzreb, and Christof M. Niemeyer\*

Artificial reconstruction of naturally evolved principles, such as compartmentalization and cascading of multienzyme complexes, offers enormous potential for the development of biocatalytic materials and processes. Due to their unique addressability at the nanoscale, DNA origami nanostructures (DON) have proven to be an exceptionally powerful tool for studying the fundamental processes in biocatalytic cascades. To systematically investigate the diffusion-reaction network of (co)substrate transfer in enzyme cascades, a model system of stereoselective ketoreductase (KRED) with cofactor regenerating enzyme is assembled in different spatial arrangements on DNA nanostructures and is located in the sphere of microbeads (MB) as a spatially confining nano- and microenvironment, respectively. The results, obtained through the use of highly sensitive analytical methods, Western blot-based quantification of the enzymes, and mass spectrometric (MS) product detection, along with theoretical modeling, provide strong evidence for the presence of two interacting compartments, the diffusion layers around the microbead and the DNA scaffold, which influence the catalytic efficiency of the cascade. It is shown that the microscale compartment exerts a strong influence on the productivity of the cascade, whereas the nanoscale arrangement of enzymes has no influence but can be modulated by the insertion of a diffusion barrier.

## 1. Introduction

Inspired by evolutionarily optimized, highly efficient principles of nature, the organization of catalytically active biomolecules at the nano- and micrometer length scale offers new possibilities for controlling reactions in biocatalysis and synthetic chemistry.<sup>[1,2]</sup> In particular, the concept of compartmentalization, in which different cooperating catalytically active units are arranged in spatially confined reaction volumes to achieve regulation of overall activities or to allow channeling of substrates, is extensively used in natural biological systems and serves as a source of innovation for research and development in biotechnology.<sup>[3–6]</sup> Although the underlying mechanisms of the compartmentalization phenomenon are not yet comprehensively understood, Hess and coworkers have already been able to develop design principles for optimized compartmentalized enzyme cascade reactions, primarily through modeling.<sup>[7]</sup> Nevertheless, fundamental studies as well as practical applications of compartmentalization require physical reaction systems that allow spatial confinement of the diffusion of protein and

substrate/product molecules on different length scales and ideally also allow the reuse of expensive biocatalyst molecules.

A significant approach to create confined diffusion spaces is based on the immobilization of enzymes on suitable support materials, such as proteins, polymers, nano- and microparticles, or nucleic acids, which can be used as interfaces to study coupled enzyme reactions.<sup>[6,8]</sup> Of these support materials, nucleic acids offer distinct advantages, as an ever-growing diversity of methods exists for targeted protein bioconjugation<sup>[9]</sup> and, most importantly, as nucleic acid supports enable unique precision for site-directed immobilization at the lower nanometer length scale. While this has already been achieved by specific Watson–Crick base pairing of nucleic acid-enzyme conjugates with linear single-stranded (ss)DNA templates<sup>[10,11]</sup> or by assembly of enzymes bearing specific binding tags, for example, Zinc-finger or aptamer-binding domains, on intracellular double-stranded (ds)DNA<sup>[12]</sup> or RNA,<sup>[13–15]</sup> the easy access to complex 2D and 3D DNA scaffolds by the scaffolded DNA origami method<sup>[16]</sup> has opened entirely new possibilities to build the multienzyme

S. Kröll, T. Burgahn, K. S. Rabe, C. M. Niemeyer  
Karlsruhe Institute of Technology (KIT)  
Institute for Biological Interfaces (IBG 1)  
Hermann-von-Helmholtz-Platz 1, D-76344 Eggenstein-Leopoldshafen,  
Germany  
E-mail: niemeyer@kit.edu

M. Franzreb  
Karlsruhe Institute of Technology (KIT)  
Institute of Functional Interfaces (IFG)  
Hermann-von-Helmholtz-Platz 1, D-76344 Eggenstein-Leopoldshafen,  
Germany

 The ORCID identification number(s) for the author(s) of this article can be found under <https://doi.org/10.1002/smll.202304578>

© 2023 The Authors. Small published by Wiley-VCH GmbH. This is an open access article under the terms of the Creative Commons Attribution-NonCommercial-NoDerivs License, which permits use and distribution in any medium, provided the original work is properly cited, the use is non-commercial and no modifications or adaptations are made.

DOI: 10.1002/smll.202304578

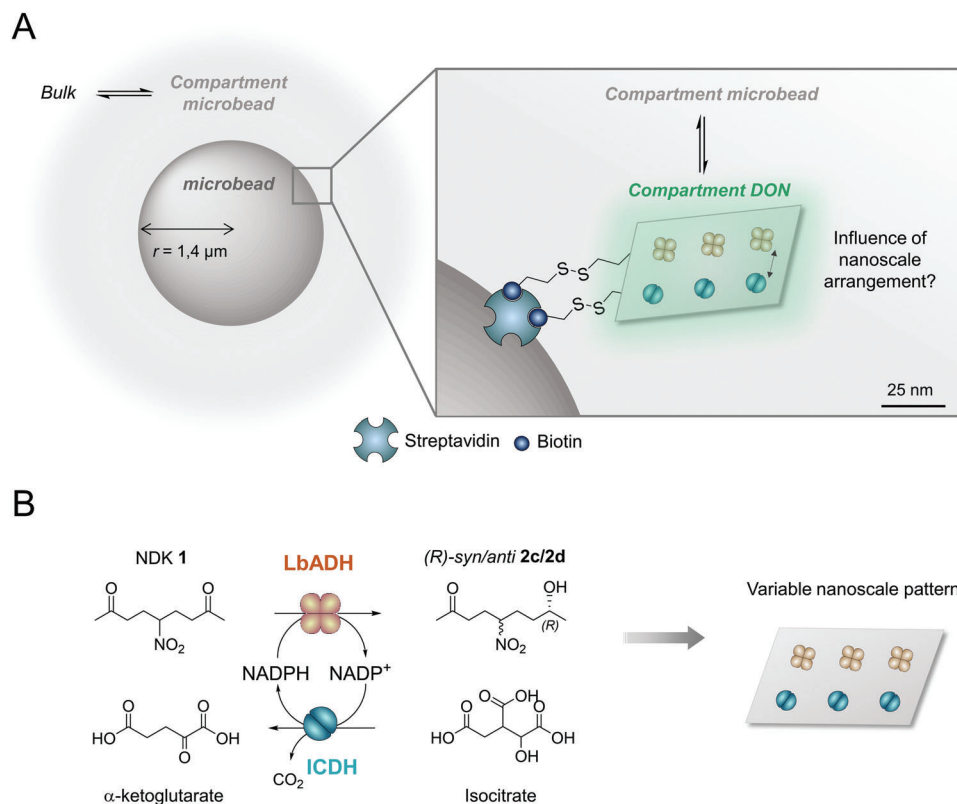


**Figure 1.** Spatially confined diffusion-reaction network of a biocatalytic cascade consisting of the ketoreductase LbADH (yellow) and the cofactor-regenerating enzyme ICDH (blue). A) Schematic of hypothetical confinements on two different length scales within the studied system, where different nanoscale arrangements of enzymes on DON are positioned via biotin bridges in the microscale compartment of magnetic microspheres ( $r = 1.4 \mu\text{m}$ ). B) Reaction network of the enzyme cascade from the (*R*)-selective LbADH and the cofactor-regenerating ICDH.

complexes in vitro. Since DNA origami nanostructures (DON) allow the immobilization of proteins with a positional accuracy of  $\approx 6 \text{ nm}$ , it is not surprising that numerous studies have been conducted to explore DON-based enzyme cascades,<sup>[15,17–24]</sup> which often report a significant impact of the intermolecular distance between individual enzymes of the cascade on the overall catalytic productivity.<sup>[25]</sup> However, the underlying reasons leading to the altered cascade performance remain controversial. Possible mechanistic explanations range from the high negative surface charge of DON favoring, for example, an altered pH microenvironment or the formation of a diffusion-limiting hydration layer, over steric protection from degradation and unfolding, to direct channeling of substrates on the scaffolds.<sup>[26,27]</sup>

Another problem contributing to the lack of clarity is the large differences that have been reported even for the same pair of enzymes. For example, in the literature, increases caused by nanoscale proximity for the very well-studied enzyme cascade of glucose oxidase (GOx) and horseradish peroxidase (HRP) range from moderate 1.5-fold to strong >20-fold. It is suggested that these differences could be due to technical inaccuracies, insufficient characterization or purification of the derivatized enzymes and the assembled enzyme-scaffold complexes.<sup>[6]</sup> Since (bio)chemical modification of enzymes often leads to altered activities and stabilities, and residual free enzymes can also bias activity measurements of assembled complexes, it is of paramount importance to accurately characterize the kinetic parameters of

the free and assembled enzymes and also perform rigorous controls, which are imperative to quantify proximity effects and thus advance the field.

In addition to the multitude of possible technical inaccuracies, another relevant cause could be microscale compartmentalization effects that occur, for example, due to inadvertent agglomeration of the complexes or when microparticles are used as carriers for the DON-enzyme complexes. Although activity increases have been described for enzyme cascades immobilized on particles,<sup>[28–32]</sup> which can be attributed to compartmentalization effects, the interplay of nano- and microscale effects on biocatalytically relevant diffusion processes has hardly been investigated,<sup>[33]</sup> in particular because of the lack of robust experimental model systems. To overcome these limitations and further advance our understanding of the elusive mechanisms underlying biocatalytic diffusion-reaction networks, we report here the detailed investigation of a biocatalytic cascade consisting of a stereoselective ketoreductase (KRED) and a cofactor-regenerating enzyme arranged with nanometer precision on DON and positioned within microscale compartments of dispersed microbeads (MB) (Figure 1).

## 2. Results and Discussion

In order to study the diffusion-reaction network in the two hypothetical compartments with a robust experimental model system

that also allows for high temporal resolution in the early phases of the reaction, it was necessary to accomplish the immobilization of the enzymes as efficiently and the analytical quantification of the reaction as sensitively as possible. The need for highly efficient yet chemically mild protein immobilization techniques has led to the development of orthogonal connector systems in recent years, including the HALO/HOB- (Halo-based oligonucleotide binder)<sup>[34]</sup> and the SNAP-tag<sup>[35]</sup> systems. Both systems use genetically-encoded fusion tags on the proteins that couple with high efficiency to corresponding suicide ligands on the DON, chlorohexyl (CH) and benzylguanine (BG) ligands for the HOB tag and SNAP-tag, respectively, in a site-specific and orthogonal manner. Here, we chose this approach for immobilizing the enzymes on DON because the high performance of this type of DON decoration had been demonstrated in numerous examples by us<sup>[19,34–40]</sup> and others.<sup>[21,41–43]</sup> Furthermore, we developed an HPLC method coupled with highly sensitive mass spectrometry (MS) detection to optimize accurate time-resolved quantification of reaction products and gain insights into the reaction-diffusion network effects of spatially organized biocatalytic cascades. Using this experimental model, we investigated a series of biocatalytic nanostructures with different immobilization patterns and positioned them in the microcompartment of dispersed magnetic beads. It was found that the nanoscale compartmentalization is only to a small extent affected by the distance between the enzymes and the insertion of diffusion barriers, while the microscale confinement space exerts a stronger influence on the biocatalytic efficiency of the cascade.

## 2.1. Design and Assembly of the Experimental Model System

Building on our previous studies on KRED-based DNA origami nanostructures,<sup>[35,39,40]</sup> we here investigated a cascade consisting of the tetrameric (*R*)-selective alcohol dehydrogenase LbADH (EC 1.1.1.2) from *Lactobacillus brevis* and the dimeric isocitrate dehydrogenase ICDH (EC 1.1.1.42) from *Bacillus subtilis*. The reaction scheme in Figure 1B shows that LbADH catalyzes the reduction of the model substrate 5-nitrononae-2,8-dione **1** (NDK) in a stereoselective manner to form (*R*)-*syn*/*anti*-hydroxyketones **2c/d** (d.r.  $\approx$  60 : 40).<sup>[44]</sup> To enable the carbonyl reduction of NDK, the cofactor NADPH is provided by ICDH by being continuously regenerated from NADP<sup>+</sup> by oxidation of isocitrate.

For efficient ligation of the enzymes with functionalized DON, LbADH was N-terminally fused to the HOB-tag,<sup>[34]</sup> while ICDH was C-terminally equipped with the engineered SNAP variant<sup>[35]</sup> to yield HOB-LbADH or ICDH-SNAP, respectively. The fusion proteins were expressed heterologously in *Escherichia coli* and purified by Ni-NTA-affinity chromatography (Figure S1, Supporting Information). To investigate the influence of the different nano- and microscale compartments on the reaction-diffusion network of the LbADH-ICDH cascade, nanoscale arrangements were designed to allow both separate or co-arrangement of the enzymes on DON, the spacing between the different enzymes, and the insertion of a non-catalytic barrier protein. For this purpose, a rectangular DON of approximately 70 × 100 nm<sup>2</sup> dimensions was used,<sup>[45]</sup> which was equipped with three distinguishable CH- and BG-ligands additionally to cleavable biotin (Btn)-linkers. The latter served to enable the immobilization of the enzyme-DON con-

structs on streptavidin (STV)-coated magnetic microbeads as well as the bead-assisted purification of the DON constructs.<sup>[39]</sup> For details on the DON designs, see Figure S2, Supporting Information.

To quantify the enzyme occupancy densities, DON in solution was incubated with 25 equivalents (eq.) of HOB-LbADH and ICDH-SNAP fusion proteins, the resulting constructs were purified by magnetic microbead extraction, cleaved from the beads with the reducing agent dithiothreitol (DTT), and the amounts of immobilized enzyme were determined by AFM analysis. Typical occupancy densities averaging 84% for HOB-LbADH and 75% for ICDH-SNAP were found (Figure S3, Supporting Information), which were in agreement with previous work<sup>[35]</sup> and ensured that sufficient amounts of enzyme could be immobilized for subsequent cascade performance analyses.

## 2.2. Kinetics of Individual Cascade Enzymes

To gain detailed insight into the mechanisms of nanoscale enzyme cascades, the components involved were precisely quantified and extensively characterized. The investigation of the kinetic parameters of the individually immobilized biocatalysts of the cascade is particularly important, as it was known from previous studies that DON immobilization of individual KREDs can lead to significantly altered enzymatic activity,<sup>[46]</sup> and that the increase in activity of one enzyme should increase the productivity of the entire cascade.<sup>[27]</sup> Therefore, both cascade enzymes were first examined individually with respect to their kinetic parameters on the microbeads and DNA origami before analyzing the activity of the co-assembled cascade. Since both reactions catalyzed by ADHs and ICDHs are multisubstrate reactions for which sequential mechanisms have been proposed,<sup>[47,48]</sup> all reactions were performed under pseudo-first order conditions. This means that the concentration of one of the substrates (NDK/NADPH or isocitrate/NADP<sup>+</sup>) was varied while the other was added in at least equimolar amount or in excess. All kinetic measurements were performed in triplicate, with enzyme concentrations determined immediately before each experiment. Michaelis–Menten parameters  $K_m$  and  $k_{cat}$  were identified by linear regression of the measurement curves and fitting the initial reaction rates versus substrate concentrations.<sup>[49]</sup> The experimentally determined data summarized in Table S1, Supporting Information, are briefly discussed below.

The catalytic properties of ICDH-SNAP were determined by fluorescence spectroscopy detection of NADPH (Figure S4, Supporting Information). We found comparable values for  $K_m$  ( $\approx$ 38  $\mu$ M or  $\approx$ 37  $\mu$ M) and  $k_{cat}$  ( $\approx$ 12.6 or 9.6 s<sup>-1</sup> for the monomeric unit of the dimer) for isocitrate and NADP<sup>+</sup>, respectively, indicating that the enzyme converted the substrate isocitrate almost equally efficiently as the cofactor NADP<sup>+</sup> (Table S1, Supporting Information). The kinetics of HOB-LbADH for the crucial cofactor NADPH were determined using an absorption-based assay (Figure S5, Supporting Information), revealing a  $K_m$  value of  $\approx$ 190  $\mu$ M and a  $k_{cat}$  value of 2 s<sup>-1</sup> for the monomeric unit of the tetramer (Table S1, Supporting Information). Compared to literature-described kinetic parameters of LbADH ( $K_m \approx$  40  $\mu$ M,  $k_{cat} \approx$  38 s<sup>-1</sup>)<sup>[47]</sup> the HOB variant used here showed decreased activity and affinity toward NADPH, which could be attributed

to the different assay conditions and/or the fused HOB tag domain. In fact, since it is well known that terminal fusion tags can exert a significant influence on enzyme activity,<sup>[50–52]</sup> the effect of the HOB domain is likely to be of substantial importance for this divergence due to its considerable size of 297 amino acids.<sup>[15,34]</sup> Overall, this initial kinetic characterization showed that HOB-LbADH has an approximately 30-fold lower catalytic efficiency in terms of NADP(H) turnover (usually described as  $k_{\text{cat}}/K_{\text{m}}$ ),<sup>[53]</sup> compared to ICDH-SNAP. This indicates that the co-factor NADPH is provided by ICDH faster than it can be consumed by the LbADH reaction, so that an equimolar cascade is not limited by a lack of NADPH but that LbADH is the rate-determining enzyme.

To investigate the catalytic parameters of HOB-LbADH for the substrate NDK 1, an alternative assay had to be developed to improve the dynamic range and sensitivity of NADPH detection of spectrophotometric analysis. To this end, a highly sensitive HPLC-MS method was established, which allowed for the sensitive and direct quantification of the hydroxyketone reaction products in a time-resolved manner (Figure S6, Supporting Information). With this method, the reaction products could be detected after only 30 s of reaction time, which corresponds to femtomole amounts of hydroxyketones. In comparison, the previously used standard HPLC method with absorption-based diode array detection,<sup>[44]</sup> can only detect hydroxyketone amounts in the nanomole range, for which reaction times of several hours are required. The tremendous sensitivity of the new HPLC-MS method is not only useful for improved characterization of the individual enzymes, but also allowed for the first time to study the kinetic effects and rates in the early stages of the reaction, which can differ significantly from the parameters when the cascade has reached steady-state equilibrium. In the case of isolated HOB-LbADH, the assay showed that this enzyme has an unproductive NADPH conversion ( $k_{\text{cat}}$  for NDK and NADPH of 0.3 and 2 s<sup>-1</sup>, respectively), a phenomenon well known in the literature for ADH ketoreductases (see also Table S1, Supporting Information).<sup>[47,54]</sup>

We next evaluated the influence of enzyme immobilization on the microbeads as well as on the negatively charged DNA surface for the individual enzymes. For this purpose, ICDH-SNAP or HOB-LbADH, respectively, were immobilized separately either on DON (@DON), directly on the microbeads (@MB), or on DON bound to microbeads (DON@MB). For ligation on DON, we employed designs with either three BG- or CH-ligands which were loaded with the enzymes. For direct immobilization on the microbeads, ICDH-SNAP was bound using a BG-oligonucleotide anchored to the beads by a complementary Btn-modified oligonucleotide. HOB-LbADH was immobilized on the microbeads by using a flexible CH-PEG-biotin linker. Immobilization of the enzymes in the DON@MB samples was accomplished by first binding the DON on the beads using Btn-bridges, then loading it with ICDH-SNAP or HOB-LbADH, and subsequently removing unbound enzyme by magnetic separation. To account for the possible nonspecific binding of the enzymes to DON or MB, negative controls were performed by, on the one hand, treating a DON without BG- or CH-binding sites analogous to the enzyme loading protocol of DON@MB (control 1) and, on the other hand, incubating MB without the corresponding BG- or CH-linker with the enzymes (control 2).

**Table 1.** Kinetic parameters of free and immobilized ICDH-SNAP for isocitrate and HOB-LbADH for NDK, respectively. Activity was determined by fluorescence spectroscopy measurement for ICDH or HPLC-MS for LbADH under pseudo-first order conditions. The  $k_{\text{cat}}$  was calculated based on the amount of enzyme used and is given per one functional unit of the multimeric enzymes.

|                    | ICDH-SNAP—Isocitrate conversion  |   | HOB-ADH—NDK conversion         |  |
|--------------------|----------------------------------|---|--------------------------------|--|
|                    | $K_{\text{m}}$ [ $\mu\text{M}$ ] | $k_{\text{cat, Dimer}}$ [ $\text{s}^{-1}$ ] | $K_{\text{m}}$ [ $\text{mM}$ ] | $k_{\text{cat, Tetramer}}$ [ $\text{s}^{-1}$ ] |
| Free               | 37.9 ± 2.9                       | 16.7 ± 0.2                                  | 3.9 ± 0.3                      | 1.28 ± 0.05                                    |
| DON-immobilized    | 37.1 ± 3.9                       | 15.9 ± 0.3                                  | 4.2 ± 0.7                      | 1.20 ± 0.08                                    |
| MB-immobilized     | 37.4 ± 6.2                       | 16.1 ± 0.6                                  | 3.6 ± 0.6                      | 2.24 ± 0.12                                    |
| DON@MB-immobilized | 34.5 ± 4.7                       | 15.8 ± 0.6                                  | 4.3 ± 0.5                      | 2.84 ± 0.15                                    |

Enzyme activities were determined by fluorescence spectroscopy detection of NADPH (ICDH) or HPLC-MS analysis of hydroxyketones (LbADH). The above controls showed almost no activity and were subtracted from the corresponding samples to calculate normalized initial rates of enzyme activity. Furthermore, all samples were quantitatively analyzed by Western blot after activity measurement (Figures S8,S9, Supporting Information) in order to account for potentially varying enzyme amounts, and the obtained  $k_{\text{cat}}$  values were corrected by the actually present enzyme amounts.

The measurements revealed no significant differences in the  $K_{\text{m}}$  values of ICDH between the free diffusing and the immobilized enzyme (Table 1). Likewise, the  $k_{\text{cat}}$ -values of the free and immobilized ICDH, regardless of ligation on DON, microbeads or DON@MB, were in a comparable range of  $\approx 16 \text{ s}^{-1}$ , indicating that the activity of ICDH-SNAP was not affected by immobilization. The affinity of HOB-LbADH was barely affected by immobilization, as indicated by comparable  $K_{\text{m}}$  values of  $\approx 4 \text{ mM}$ . Also, DON immobilization did not appear to have a significant effect on the activity of the enzyme, as indicated by a comparable  $k_{\text{cat}}$  value of  $1.20 \text{ s}^{-1}$ , which was close to the value of the free enzyme of  $1.28 \text{ s}^{-1}$ . In contrast, increased activities were observed for both MB- and DON@MB-immobilized LbADH, whose  $k_{\text{cat}}$  values were approximately 75% and 122% higher than those of the free enzymes, respectively (Table 1). These data suggested that immobilization of LbADH in the microbead compartment has a significant effect, while binding on DON has only a minor effect on enzyme activity. As discussed below, this could be due to the altered local environment at the MB surface, which appears to be different from the compartmentalized reaction space of the DON.

We observed that the increase in activity of LbADH immobilized @MB or DON@MB occurred virtually unchanged even in the substrate saturation region, that is, at maximum reaction rate (Figure S9A, Supporting Information). Therefore, the increase in activity appeared to be due to a direct influence on the catalytic reactivity, and not on transient diffusion processes, such as a favored substrate transfer. The significant difference in  $k_{\text{cat}}$  of @DON and DON@MB samples further indicated a synergistic effect by immobilization in the compartments of DON and MB, which is consistent with previous observations obtained for comparable but different ligation chemistry based

DON@MB-LbADH systems.<sup>[40]</sup> Therein, a SpyCatcher-modified LbADH showed 40% higher activity than the free enzyme upon immobilization. Thus, the results indicate that the type of immobilization can have a substantial impact on the activity of immobilized enzymes and highlight the importance of a comprehensive characterization of individual enzymes before considering interacting cascades of immobilized enzymes.

An increase in catalytic activity as a result of immobilizing enzymes has been frequently described for nanoscale systems, such as DNA surfaces and nanoparticles, as well as for microscaled compartments.<sup>[6]</sup> Common explanations include compartmentalization effects, such as an altered pH microenvironment or the formation of a hydration layer, protection from degradation, electrostatic interactions of substrates with the scaffolds or a high local density of enzyme entities.<sup>[20,55,56]</sup> For example, the influence of a reduced pH in close proximity to the DON surface was proposed as an explanation for the activity increase of scaffolded GOx-HRP cascade.<sup>[57]</sup> In a recently published study, however, the local pH shift near the surface of the DNA scaffold was found to be only a small pH difference of 0.8.<sup>[58]</sup> This result suggests no general influence of pH on the activity differences, which is in good agreement with our previous study on KRED-DON constructs.<sup>[40]</sup> As ICDH showed a maximum activity at pH 9 and only a low relative activity at pH 5 (Figure S10, Supporting Information), it can be assumed that the local pH change due to the negatively charged surface most likely does not play a significant role in the activity enhancement of the LbADH/ICDH system. Other explanations include the stabilization of enzymes by the formation of a hydration layer,<sup>[20,24]</sup> which however, is also presumed to be considerably thin with only a few angstroms.<sup>[59]</sup> Furthermore, electrostatic interactions between substrates, carriers, or protein domains, allosteric effects, and locally increased enzyme/substrate concentrations have also been reported in the literature to increase the activity of immobilized enzymes.<sup>[27,56,60]</sup> By conjugating an ADH with a strongly charged protein, it was shown that the addition of charges near the active site affected the local ionic strength and pH and influenced the enzyme activity.<sup>[61]</sup> Such charge differences could possibly result from the strongly negatively charged DNA surface concentrated within the microbead environment, thus affecting the activity of LbADH. Furthermore, it was observed that the activity of a lactate dehydrogenase was enhanced by binding to quantum dots, and the magnitude of the enhancement was even dependent on the size of the particle.<sup>[62]</sup> This effect was attributed to an increase in stability by assuming that the immobilization predominantly causes the tetrameric structure of the enzyme to be present, whereas in free solution the dissociated form is present. Based on these studies, it can be hypothesized that the intrinsic reactivity of LbADH is also increased by charge states near the enzyme, possibly with additional conformational stabilization, upon immobilization on DON in the microbead sphere.

### 2.3. Kinetics of the LbADH-ICDH Cascade

The above studies indicated that the activity of the HOB-LbADH was still about fivefold lower than that of the ICDH-SNAP despite the increase due to immobilization on the microbeads loaded with DON (Table 1). This suggested constant and effi-

cient cofactor regeneration within the cascade, and thus provided a solid basis for the subsequent investigation of possible cooperative effects of DON structures and the microbeads on the overall cascade productivity. For this purpose, HOB-LbADH and ICDH-SNAP were immobilized in different combinations of DON structures and microbeads (Figure 2A). DON equipped with either three CH-ligands for HOB-LbADH ( $A_3$ ) or three BG-ligands for ICDH-SNAP ( $I_3$ ) were used to immobilize the cascade enzymes on separate DON, which were then either bound to separate microbeads ( $A_3$ -DON@MB +  $I_3$ -DON@MB, blue in Figure 2A) or to the same microbeads ( $A_3$ -DON +  $I_3$ -DON@MB, green). For co-assembly of the cascade on DON@MB, a DON design equipped with three CH- and three BG-ligands was used ( $A_3I_3$ -DON@MB, yellow). All DON-based samples were prepared with 25 eq. each of HOB-LbADH and ICDH-SNAP per available ligand, and unbound enzyme was removed by magnetic separation after assembly. For comparison, freely diffusing enzymes were examined, and a negative control of DON without binding sites was used to account for nonspecific binding of the enzymes.

Cascade reactions were started by adding a reaction solution containing 10 mM isocitrate, 0.5 mM NDK, and 0.5 mM NADP<sup>+</sup>. Because the overall rate of the reaction depends on NADPH production by ICDH and its action on LbADH, the NADP<sup>+</sup> and NDK concentrations were intentionally reduced to gain insight into the effects of co-immobilization and potential mass transfer limitations. Reactions were monitored between 0.5 and 120 min via HPLC-MS (representative plots of product concentration vs. time are shown in Figure S11, Supporting Information). To compare the reaction rates of the different samples, the specific catalytic productivity (turnover number, TON) was determined. The TON for each reaction was calculated from the enzymatic turnover of NDK 1 into the specific hydroxyketones **2c/d** minus the control sample and normalized by the amount of HOB-LbADH in the corresponding time unit. For this purpose, Western blot analyses with calibration standards were performed to determine the concentrations of both HOB-LbADH and ICDH-SNAP (Figure S12, Supporting Information). Consistent with other studies on DNA scaffold-based cascades,<sup>[24]</sup> only the actual concentrations of HOB-LbADH present in the samples were used to calculate TON because, as shown above, LbADH is the rate-determining enzyme of the cascade.

As shown in Figure 2B,C, the observed dynamics of the specific TON values revealed striking differences between the free diffusing enzymes and the different immobilized cascade constructs. A significant increase in TON was observed in all samples in the range of 0.5–2.5 min, presumably due to the initial low NADPH concentration. Interestingly, the freely diffusing enzymes exhibited significantly higher productivity in the very early phase of the reaction up to 2.5 min, whereas the cascades on microsphere DON did not reach comparable TON values until 2.5 min (Figure 2C). Moreover, the free enzymes showed constant TON values starting at  $\approx$ 5 min, suggesting that steady-state equilibrium was already reached at early stages of the reaction. In contrast, the TON values of all immobilized DON@MB cascade variants increased significantly from 5 min onward and reached their maxima after 60 min, which were, however, significantly higher than that of the free enzymes. It should be pointed out here that the reactions have a characteristic initial phase up to

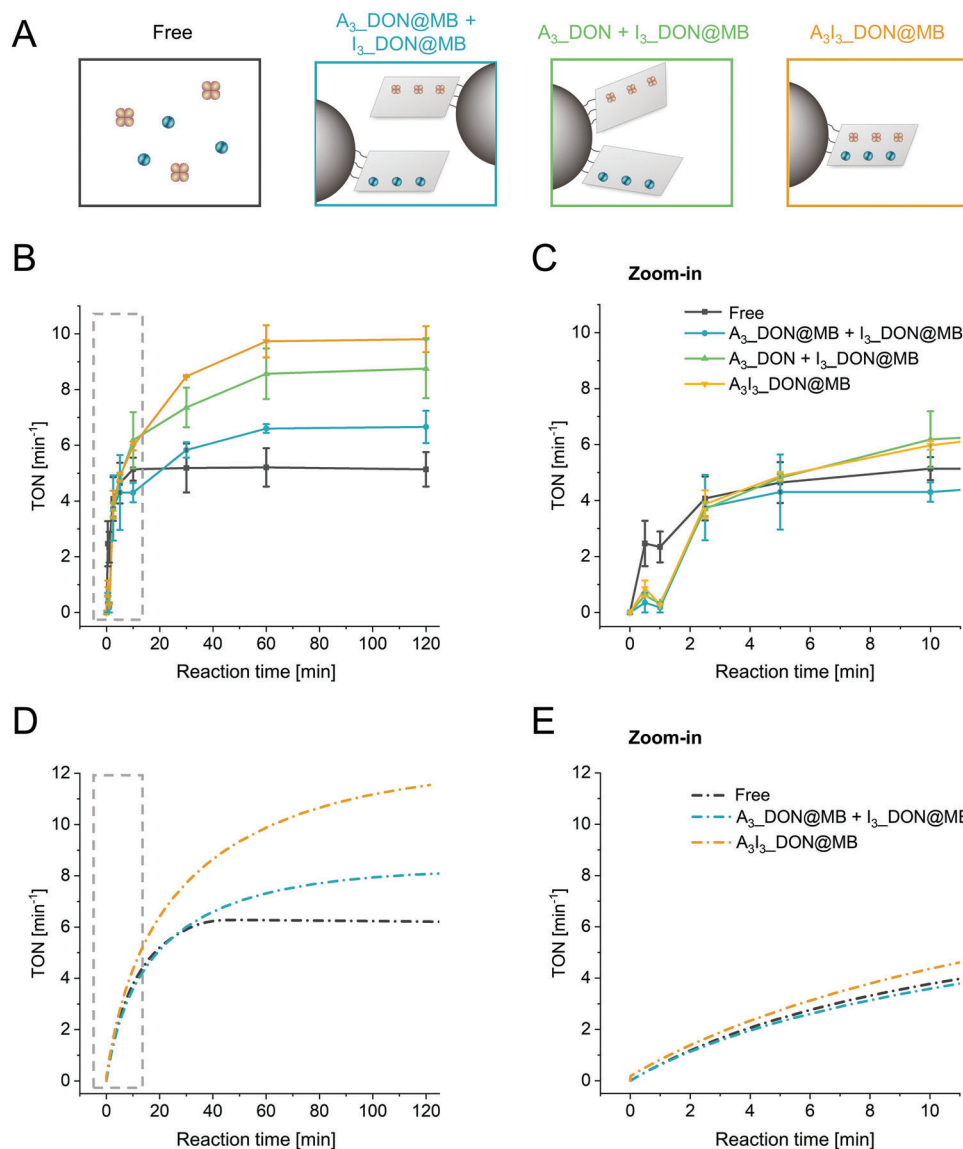


**Figure 2.** Catalytic productivity of the LbADH-ICDH cascade immobilized on different scaffolding systems. A) Schematic representation of freely diffusing enzymes, immobilized on separate DON and microbeads ( $A_3\_DON@MB + I_3\_DON@MB$ ), on separate DON on the same microbead ( $A_3\_DON + I_3\_DON@MB$ ) or co-immobilized on DON ( $A_3I_3\_DON@MB$ ). Note that the illustration is not to scale (microbeads  $r = 1.4 \mu\text{m}$  and DON  $100 \times 70 \text{ nm}$ ). B,C) Comparison of TON values as a function of reaction time with (C) as a zoom-in of the initial 10 min. Sample size ( $n$ ):  $n \geq 2$ ; All error bars represent the standard deviation (SD). D,E) Comparison of TON values obtained via modeling as a function of reaction time with (E) zoom-in of the first 10 min. It should be noted that the modeling of samples in which immobilization is realized on different DON but the same bead ( $A_3\_DON + I_3\_DON@MB$ ) cannot be distinguished from  $A_3I_3\_DON@MB$  due to the limited spatial resolution of the COMSOL model. Therefore, the green curve is not shown.

about 2.5 min, which is characterized by similar increasing TON values. This can be explained by the initial low NADPH concentrations, as the reaction starts with the conversion of  $\text{NADP}^+$  to NADPH, which is then consumed by LbADH for the conversion of NDK. However, the real productivity of each configuration is only visible in the quasi-stationary state. Due to this characteristic initial phase of the reaction, where the cascade has not yet reached the equilibrium, differences from the immobilization on the maximum productivity can only be reliably compared at later stages of the reaction ( $\approx 60 \text{ min}$ ).

Immobilization of the two enzymes on separate beads ( $A_3\_DON@MB + I_3\_DON@MB$ ) resulted in only 25% in-

creased TON at the reaction maximum compared to the free enzymes, although the individually immobilized LbADH on MB-bound DON structures exhibited 122% increased activity (Table 1). This indicates delayed cofactor transport, as the produced NADPH must diffuse out of the microenvironment of the ICDH-loaded bead and enter the compartment of LbADH-functionalized beads. In contrast, the catalytic productivity of the sample containing both enzymes in the same bead compartment ( $A_3\_DON + I_3\_DON@MB$ ) reached an increased value of about 70%, as compared to the free enzymes. However, the highest catalytic productivity was observed for the co-immobilized cascade ( $A_3I_3\_DON@MB$ ) with an approximately 100% increase in

activity compared to the free enzymes. This could be taken as a strong indication of the presence of two compartments, on the one hand the environment of the microspheres and on the other hand, although to a lesser extent, the environment of the DNA surface, the spatial interaction of which could cause a physico-chemical environment favorable to the cascade.

To gain a deeper understanding of the effects of compartmentalization on cascade productivity, a simplified Finite Element Model (FEM) of the system was developed (for details, see Appendix, Supporting Information). The modeling could be used to compare the microscale effects, that is, between samples of freely diffusing enzymes,  $A_3\_DON@MB + I_3\_DON@MB$  and  $A_3I_3\_DON@MB$ . Immobilization on different DON but the same bead ( $A_3\_DON + I_3\_DON@MB$ ) could not be distinguished from  $A_3I_3\_DON@MB$  due to the limited spatial resolution of the COMSOL model. The system of LbADH and IDCH was implemented with the respective substrates, cofactors, and products involved, all of which were considered stable under the used conditions and over the analyzed reaction time (for details, see Appendix, Supporting Information). Based on the hypothesis that the charged  $NADP^+$  could retard through electrostatic interactions and, in particular, temporary adsorption to the microbead surface and potentially also on the strongly negatively charged DON surface, thus decelerating regeneration by ICDH, a much slower effective diffusion velocity of  $NADP^+$  was assumed and TON values could be modeled. As shown in Figure 2D, qualitatively comparable curves to the experimental data in the different compartments were obtained, where the productivity of  $A_3\_DON@MB + I_3\_DON@MB$  (blue) was 33% and  $A_3I_3\_DON@MB$  (yellow) about 100% (higher than the free enzymes. Quantitatively, the TON values were also comparable upon reaching the quasi-stationary state (e.g., free diffusing cascade:  $5.05 \text{ min}^{-1}$  experimentally vs  $6.25 \text{ min}^{-1}$  in the model). Analogous to the experimental data, the freely diffusing cascade reached the maximum reaction velocity faster than the cascades immobilized on beads and DON, even though the quasi-stationary state was reached only after  $\approx 30$  min in the model, compared to  $\approx 10$  min in the experimental data. These differences could be due to variations in the kinetic parameters of the individual enzymes, which could have resulted from the Michaelis–Menten fit of the real data points. It was also evident from the model that the productivity of the free enzymes in the initial phase of the reactions was between the TON values of the separately and co-immobilized cascade at 5–10 min (Figure 2E). In contrast, the differences observed experimentally in the very early stages of the reaction at 0.5–2.5 min could not be reproduced with the model. We hypothesize that this is due to the complex environment in the DON and microsphere diffusion layers caused by the DON attached to the microsphere surface, which the model could not represent due to its limited spatial resolution of  $\approx 0.4 \mu\text{m}$  in the diffusion layer surrounding the microbeads. For a brief review of diffusion layers and modeling with COMSOL, see Appendix, Supporting Information.

Overall, the model as well as the experimental data provided strong evidence that the environment generated by the microbead sphere has a significant impact on the productivity of LbADH and thus the cascade. The concept of such a stagnant fluid layer has been frequently described in literature, and of-

ten a resulting locally increased concentration of intermediates has been assumed. For example, Arrio-Dupont et al. observed an activity increase for the coupled reaction of an aspartate aminotransferase and malate dehydrogenase co-immobilized on the surface of a collagen film.<sup>[63]</sup> This was attributed to the intermediate oxaloacetate being preferentially consumed in the diffusion layer near the collagen film without diffusively escaping into the surrounding solution. Jia et al. reported a two-fold activity increase of the GOx-HRP cascade co-immobilized on polystyrene nanoparticles ( $\approx 200 \text{ nm}$ ) compared to a mixture of separately immobilized enzymes, which was ascribed to a preferential substrate transfer.<sup>[64]</sup> Similar results were also described in lectin-agglutinated GOx-HRP aggregates ( $\approx 1 \mu\text{m}$ ).<sup>[65]</sup> Moreover, in the context of biomimetic cascades of glycolytic enzymes, it was observed that co-immobilization of enzymes on the same particle efficiently catalyzed a sequential reaction, with individual enzymes also showing significantly increased activity due to immobilization.<sup>[28]</sup> Similarly, an increased productivity was observed in 10-step glycolytic cascade on nanoparticles, which was attributed to spatial channeling of intermediates within the hydration layer of proteins at the particle surface.<sup>[30]</sup> In addition, a recently published study further investigated the dependence of the colocalization effect on GOx-HRP cascades on microscale beads.<sup>[60]</sup> Here, the enzymes were placed on different microparticles via DNA interaction and an accelerated cascade reaction was observed, which was significantly more pronounced on larger ( $\approx 5\text{--}8 \mu\text{m}$ ) than on smaller particles ( $0.55 \mu\text{m}$ ). Based on reaction-diffusion modeling, it was shown that the colocalization effect resulted from an initial  $H_2O_2$  accumulation at the microbead surface and thus provided first theoretical approaches for effects arising from an interplay between nanoscale and microscale.

#### 2.4. Influence of the Nanoscale Interenzyme Distance

Since the results described above suggested that the compartment of DON leads to an additional increase in catalytic productivity, we wanted to investigate to what extent the nanoscale arrangement of the enzymes, that is, the interenzyme distance, on the DNA scaffold affects the cascade. To this end, DON designs were created on which the two enzymes were spaced at different distances of 6 nm ( $A_3I_3\_DON\text{-}6 \text{ nm}$ ), 30 nm ( $A_3I_3\_DON\text{-}30 \text{ nm}$ ), or 70 nm ( $A_2I_2\_DON\text{-}70 \text{ nm}$ ) (Figure 3A). For the 6 nm and 30 nm spacings, three BG- and CH-ligands, were used, whereas for the 70 nm spacing, only two BG- and CH-binding sites were available for enzyme immobilization due to spatial constraints. Since the experimental analysis was based on the determination of TON values, the difference between two or three interacting enzyme pairs could be considered for the comparison between values. The efficient ligation of the fusion enzymes on the designated binding sites was confirmed by AFM analysis (Figure 3B, see Figure S13, Supporting Information, for full-scale images).

To analyze the activity of the immobilized cascade, freely diffusing enzymes and a negative control were used for comparison, and the amounts of protein were subsequently quantified by Western blot analysis (Figure S14, Supporting Information), analogous to the procedure described above. In agreement with

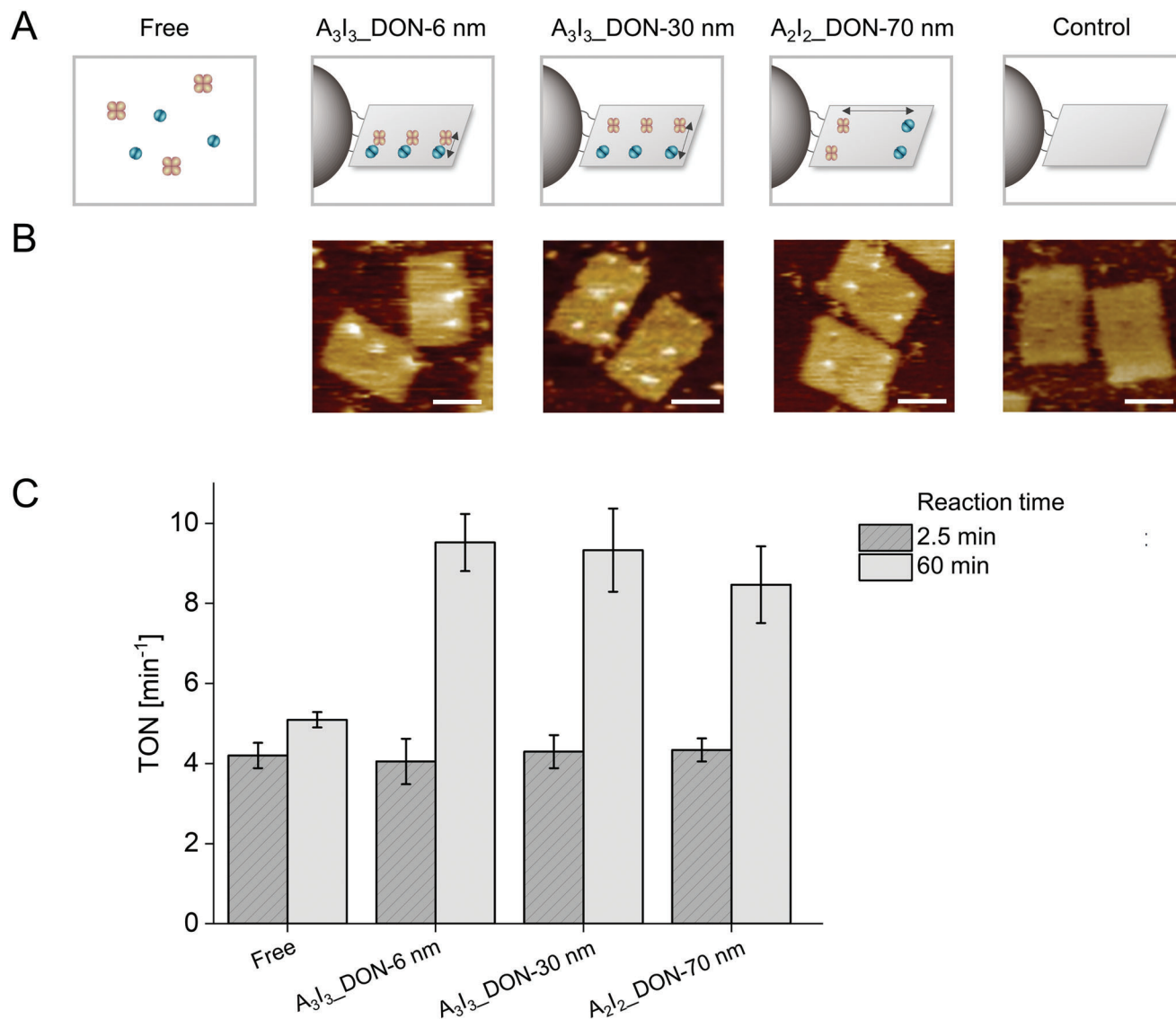


**Figure 3.** Kinetic characterization of the LbADH-ICDH cascade immobilized in various nanoscale interenzyme distances. A) Schematic representation of the freely diffusing cascade, HOB-ADH/ICDH-SNAP immobilized on DON with 6 nm ( $A_3I_3\_DON-6\text{ nm}$ ), 30 nm ( $A_3I_3\_DON-30\text{ nm}$ ), or 70 nm ( $A_2I_2\_DON-70\text{ nm}$ ) spacing and a negative control. B) Representative AFM images of the different DON constructs with immobilized HOB-LbADH and ICDH-SNAP, obtained after reductive cleavage of decorated constructs from the beads. Scale bars: 50 nm. For large-scale images, see Figure S13, Supporting Information. C) Catalytic productivity (TON) of LbADH/ICDH-based cascade reaction. Sample size ( $n$ ):  $n \geq 2$ ; All error bars represent the standard deviation (SD).

the previous data (Figure 2), kinetic analysis revealed comparable TON values for the free enzymes after 2.5 min and 60 min reaction time, again showing the rapid establishment of the quasi-stationary state (Figure 3C). Comparable TON values were obtained for the DON-immobilized cascades after 2.5 min, with a  $\approx 90\%$  higher productivity at the quasi-stationary state than that of the free enzymes after 60 min, consistent with the trends observed above. Importantly, the nanoscale arrangement of HOB-LbADH and ICDH-SNAP on the DON did not result in a significant decrease in catalytic productivity when the distance between the enzymes was increased from 6 nm to 70 nm. This was a clear indication that the observed increase in catalytic productivity in the LbADH-ICDH cascade is not due to a proximity-

based substrate channeling mechanism, but rather that the placement of the DON-immobilized cascade within the microbead sphere creates a favorable environment for the cascade reaction.

Indeed, the presence of a channeling mechanism in DNA-based cascades has often been challenged in the context of an increased turnover. In general, channeling refers to the process in which intermediates between sequential enzyme reactions are directly transferred from one active site to another without being released into the bulk solution, as realized in nature, for example, via hydrophobic channels.<sup>[2,7]</sup> For scaffolded systems, the underlying mechanisms can be considerably more complex, and also strongly depend on the chosen cascade and specific

kinetic properties of the enzymes. The initially proposed proximity-based channeling mechanism however, was found to be only effective in transient time scales and to not result in a permanent increase in cascade activity.<sup>[2,24,26,57]</sup> Our results are therefore consistent with other studies in which a generally increased activity of an enzyme cascade immobilized on DON was observed, but attributed to molecular effects of DON, such as confinement, rather than to the mere spatial proximity of the enzymes.<sup>[27]</sup> Similarly, the increase in activity described by Fu et al. for the close spatial arrangement of the immobilized GOx-HRP cascade<sup>[17]</sup> was later explained by Zhang et al. as a pH effect of the strongly negatively charged DON surface, which should increase the activity of the pH-sensitive HRP enzyme.<sup>[57]</sup> Catalytic enhancements due to immobilization on DNA scaffolds were also described for enzyme cascades aside from the popular GOx-HRP system, which, however, could not be attributed to spatial proximity of the enzymes. For example, a cascade of amylase, maltase, and glucokinase immobilized on a planar DNA origami showed an approximately 19-fold increase in activity, due to the individually increased activity of maltase on the DNA surface, that showed no dependence on the spacing of the enzymes on the structure.<sup>[24]</sup> Similarly, a cascade of a xylitol dehydrogenase and a xylulose kinase on a 3D DNA nanoscaffold showed almost no correlation between the overall activity and the spatial distance of the immobilized enzymes.<sup>[66]</sup> Since proximity alone is not sufficient to achieve channeling, alternative mechanisms such as spatial clustering of active sites have been proposed, as often shown in the context of dense packing on nanoparticle surfaces,<sup>[30,32,62,67]</sup> and discussed in several review articles.<sup>[2,6–8]</sup> In our model system, we did not find such a large increase in activity, suggesting that the density of active sites required for effective channeling has not been reached.

Although the above results described here and elsewhere consistently show that the variation of spatial distances between enzymes on a DNA nanostructure does not play a significant role in the productivity of the cascade, it remains unclear to what extent the diffusion processes in the reaction space around the DNA scaffold are restricted. Therefore, to further investigate the diffusion in the compartmentalized environment of the DON on microbeads, we conducted additional experiments similar to that performed by Fu et al. with homogeneously solubilized DON-GOx-HRP cascades.<sup>[17]</sup> They demonstrated that insertion of a non-catalytic protein (streptavidin-conjugated  $\beta$ -galactosidase) between catalytically interacting GOx and HRP enzymes resulted in an increase in the overall activity of the cascade, which was attributed to a connection of the hydrate shells of the proteins and thus faster surface-limited substrate diffusion between the closely spaced proteins. Because we suspected that the potential DNA compartment is likely to be small in size, but stabilized by the influence of the microbead sphere, we here wanted to investigate whether the beneficial interplay between DON and microbeads could be affected by a bulky protein barrier at the nanoscale between the enzymes.

To this end, we used a DON design in which additional dinitrophenyl- (DNP) ligands were positioned between the CH- and BG-ligands, to allow binding of an immunoglobulin G (IgG) antibody (150 kDa) directed against DNP. On the basis of previous work on antibody binding to ligand-decorated DON, which indicated the strongest bivalent binding of IgG at interligand

spacings of 16 nm,<sup>[68]</sup> we incorporated four DNP ligands to facilitate binding of two IgG antibodies directed against DNP between the LbADH and SNAP enzymes, which were positioned either 30 nm or 70 nm apart (**Figure 4A**). In both variants, the DNP-ligands were positioned on DON such that the distance between IgG and ICDH-SNAP was  $\approx 15$  nm. The structures were subsequently characterized by AFM. As the analysis could not be performed using the microbead-purification due to sensitivity of IgG toward the reducing agent DTT, a low excess of 3 eq. each HOB-LbADH and ICDH-SNAP as well as 2 eq. IgG per binding ligand was applied. Despite the resulting high protein background, AFM analysis suggested that all positions were accessible by the respective proteins (**Figure 4B**). Moreover, an electrophoretic analysis confirmed successful ligation of all proteins to DON (**Figure S15**, Supporting Information). Subsequent activity measurements with corresponding quantification and normalization of enzyme amounts were performed as described above (see **Figure S16**, Supporting Information, for Western blot analysis). For the freely diffusing enzymes, the presence of the IgG antibody resulted in comparable productivity of the cascade after both 2.5 and 60 min, clearly demonstrating that the IgG antibody did not exert any influence on the catalytic interactions of the enzymes. For all DON constructs, we found comparable TON values after 2.5 min (**Figure 4C**), which were quantitatively consistent with previously observed values (**Figure 3C**). This is again indicating that the cascade is not yet operating at full capacity during the characteristic initial phase of the reaction.

However, the values obtained after 60 min for the DON constructs consistently showed that insertion of the IgG antibody between the enzymes resulted in a  $\approx 23\%$  decrease in activity. This decrease was comparable to the difference observed above when comparing the cascades on different or the same bead-coupled DON (**Figure 2**,  $A_3\_DON + I_3\_DON@MB$  (green) vs.  $A_3I_3\_DON@MB$  (yellow)) and suggested that the productivity gained by nanoscale co-immobilization of the LbADH/ICDH cascade is canceled out by insertion of the bulky IgG between the enzymes. Moreover, the decrease in activity was found to be independent of the interenzyme spacing between ICDH and LbADH (30 nm vs. 70 nm), again confirming that simply placing the enzymes at different distances does not lead to increased activity on the nanometer length scale for the LbADH/ICDH cascade. These results are in contrast to the study by Fu et al., in which the insertion of a non-catalytic streptavidin- $\beta$ -galactosidase resulted in an increase in the overall activity of the cascade,<sup>[17]</sup> despite the higher weight of >500 kDa compared to the IgG molecules (150 kDa) used here. The different specific surface properties of IgG and streptavidin- $\beta$ -galactosidase could be responsible for the observed decrease in activity by limiting the access of ADH to the cofactor NADPH produced by ICDH. This could alter the nanocompartment around the DON construct in terms of its size and/or physicochemical properties, thus affecting the presumed  $NADP^+$  retardation. This hypothesis is supported by a recently published work reporting the modulation of a DON-based multi-enzyme system, in which the cascade activity could be influenced by the surface affinity of the DNA scaffold for binding substrate molecules and thereby the local accumulation or depletion of substrates.<sup>[69]</sup>

Given the complexity of the scaffold-based cascades described here, it can reasonably be expected that for a general understand-

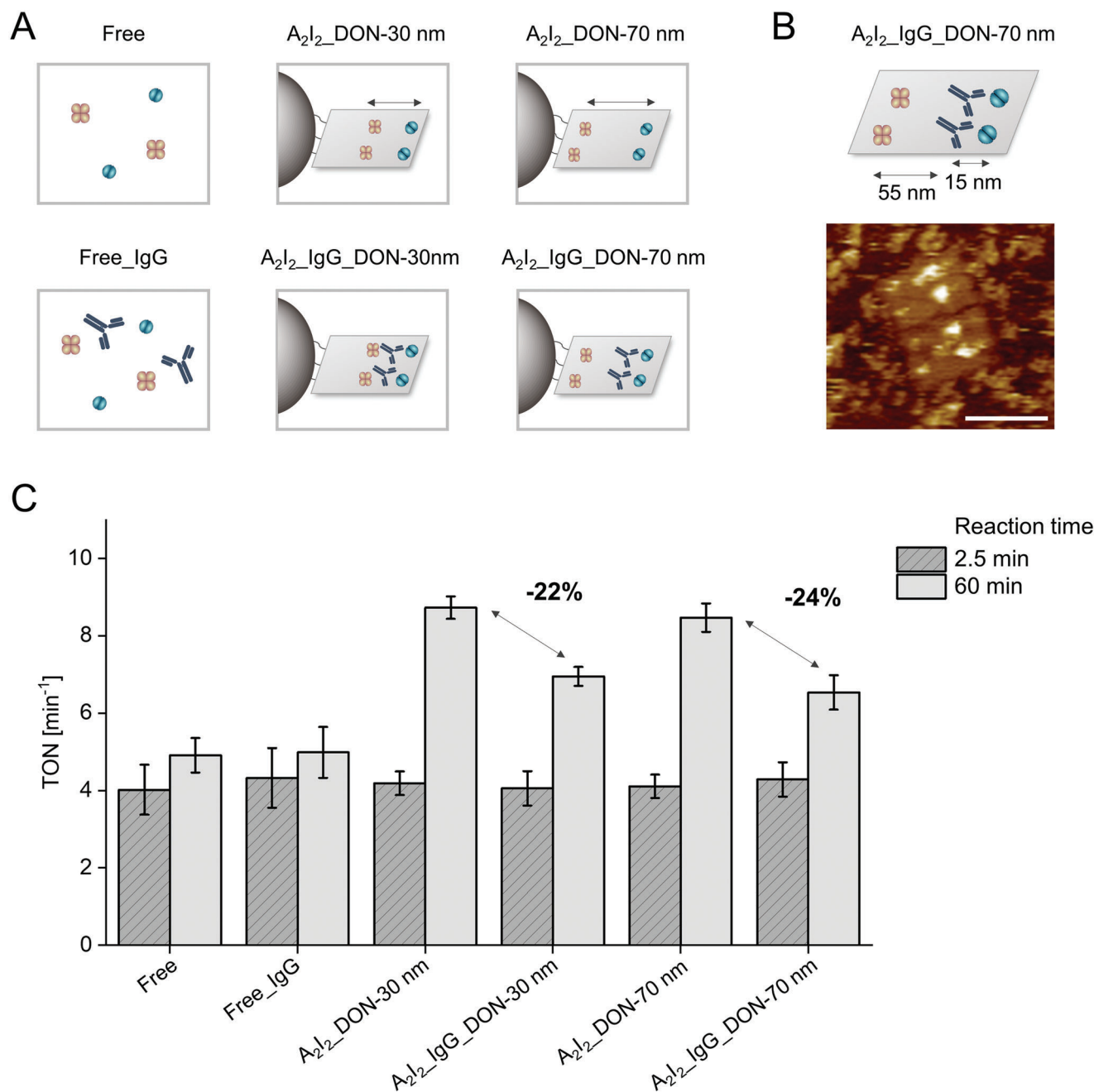


**Figure 4.** Characterization of the ADH/ICDH-based enzyme cascade with insertion of a non-catalytic anti-DNP IgG antibody. A) Schematic representation of freely diffusing cascade with HOB-ADH and ICDH-SNAP, immobilized on DON with 30 nm ( $A_2I_2$ -DON-30 nm) and 70 nm spacing ( $A_2I_2$ -DON-70 nm), respectively, and the corresponding constructs with IgG antibody. B) Representative AFM image of  $A_2I_2$ -IgG-DON-70 nm, obtained by decoration of DON with 3 eq. HOB-LbADH, 3 eq. ICDH-SNAP and 2 eq. IgG antibody per available ligand. Note that purification via microbeads was not feasible due to sensitivity of IgG toward the reducing agent DTT. Scale: 100 nm. C) Catalytic productivity (TON) of the LbADH/ICDH-based cascade reaction. Sample size ( $n$ ):  $n \geq 2$ ; All error bars represent the standard deviation (SD).

ing of such multicenter reaction-diffusion networks, more in-depth studies using different DNA scaffolds with a variety of geometries and stoichiometries as well as different enzymatic reactions with different substrates need to be conducted. The robust and precise methods presented in this study should prove useful for their systematic investigation to provide quantitative insights into nano- and microscale effects of DNA-based cascades.

### 3. Conclusion

In summary, we investigated a two-step biocatalytic reduction cascade using DNA nanostructures and microbeads as spatially confining environments. Various nanoscale arrangements were designed and cascade productivity was evaluated using sensitive methods, including HPLC-MS for precise determination of

productivity and Western blot analyses for quantifying enzyme amounts. The immobilization had minimal impact on ICDH-SNAP, but significantly increased activity of HOB-LbADH when immobilized on microbeads and microbead-bound DNA constructs. A more detailed investigation of the cooperative interplay between nano- and microscale revealed that the cascade reached its highest productivity upon co-assembly on DON in the diffusion layer of the microbead. These results indicated the presence of two compartments—the diffusion layers around the microbeads and the DNA origami scaffold—whose interplay creates a physicochemically favored environment for the cascade reaction. Theoretical modeling suggests that NADP<sup>+</sup> retention by the microbeads due to electrostatic interactions could lead to the observed different productivities. No evidence of substrate channeling based on spatial proximity on the nanoscale was found, however, the insertion of a non-catalytic protein between cascade enzymes decreased productivity, indicating an effect on the nanoscale DNA origami compartment. These findings thus provide important insights into multienzyme assemblies on nucleic acid scaffolds. The developed methodological approaches offer a powerful basis to further unravel the role of spatial organization and could lead to an exploitation of efficient principles, such as compartmentalization, for applications in biocatalysis and synthetic chemistry. This could also serve as inspiration for further improvement of other types of cascade systems, such as hybrid enzyme-metal catalysts<sup>[70]</sup> or micro- and macroporous enzyme materials.<sup>[71–74]</sup>

## Supporting Information

Supporting Information is available from the Wiley Online Library or from the author.

## Acknowledgements

This work was supported through DFG Project Ni 399/15-1 and the Helmholtz program “Materials Systems Engineering” under the topic “Adaptive and Bioinspired Materials Systems”.

Open access funding enabled and organized by Projekt DEAL.

## Conflict of Interest

The authors declare no conflict of interest.

## Data Availability Statement

The data that support the findings of this study are available from the corresponding author upon reasonable request.

## Keywords

biocatalysis, DNA nanostructures, enzyme cascades, self-assembly

Received: May 31, 2023  
Revised: August 24, 2023  
Published online:

- [1] A. Küchler, M. Yoshimoto, S. Luginbühl, F. Mavelli, P. Walde, *Nat. Nanotechnol.* **2016**, *11*, 409.
- [2] M. Vázquez-González, C. Wang, I. Willner, *Nat. Catal.* **2020**, *3*, 256.
- [3] M. C. Good, J. G. Zalatan, W. A. Lim, *Science* **2011**, *332*, 680.
- [4] A. H. Chen, P. A. Silver, *Trends Cell Biol.* **2012**, *22*, 662.
- [5] I. Wheeldon, S. D. Minter, S. Banta, S. C. Barton, P. Atanassov, M. Sigman, *Nat. Chem.* **2016**, *8*, 299.
- [6] K. S. Rabe, J. Müller, M. Skoupi, C. M. Niemeyer, *Angew. Chem., Int. Ed.* **2017**, *56*, 13574.
- [7] S. Tsitkov, H. Hess, *ACS Catal.* **2019**, *9*, 2432.
- [8] G. A. Ellis, W. P. Klein, G. Lasarte-Aragonés, M. Thakur, S. A. Walper, I. L. Medintz, *ACS Catal.* **2019**, *9*, 10812.
- [9] C. M. Niemeyer, *Angew. Chem., Int. Ed.* **2010**, *49*, 1200.
- [10] C. M. Niemeyer, J. Koehler, C. Wuerdemann, *ChemBioChem* **2002**, *3*, 242.
- [11] J. Müller, C. M. Niemeyer, *Biochem. Biophys. Res. Commun.* **2008**, *377*, 62.
- [12] R. J. Conrado, G. C. Wu, J. T. Boock, H. Xu, S. Y. Chen, T. Lebar, J. Turnsek, N. Tomsic, M. Avbelj, R. Gaber, T. Koprivnjak, J. Mori, V. Glavnik, I. Vovk, M. Bencina, V. Hodnik, G. Anderluh, J. E. Dueber, R. Jerala, M. P. Delisa, *Nucleic Acids Res.* **2011**, *40*, 1879.
- [13] C. J. Delebecque, A. B. Lindner, P. A. Silver, F. A. Aldaye, *Science* **2011**, *333*, 470.
- [14] G. Sachdeva, A. Garg, D. Godding, J. C. Way, P. A. Silver, *Nucleic Acids Res.* **2014**, *42*, 9493.
- [15] G. V. Los, L. P. Encell, M. G. McDougall, D. D. Hartzell, N. Karassina, C. Zimprich, M. G. Wood, R. Learish, R. F. Ohana, M. Urh, D. Simpson, J. Mendez, K. Zimmerman, P. Otto, G. Vidugiris, J. Zhu, A. Darzins, D. H. Klaubert, R. F. Bulleit, K. V. Wood, *ACS Chem. Biol.* **2008**, *3*, 373.
- [16] P. W. K. Rothmund, *Nature* **2006**, *440*, 297.
- [17] J. Fu, M. Liu, Y. Liu, N. W. Woodbury, H. Yan, *J. Am. Chem. Soc.* **2012**, *134*, 5516.
- [18] J. Fu, Y. R. Yang, A. Johnson-Buck, M. Liu, Y. Liu, N. G. Walter, N. W. Woodbury, H. Yan, *Nat. Nanotechnol.* **2014**, *9*, 531.
- [19] C. Timm, C. M. Niemeyer, *Angew. Chem., Int. Ed.* **2015**, *54*, 6745.
- [20] Z. Zhao, J. Fu, S. Dhakal, A. Johnson-Buck, M. Liu, T. Zhang, N. W. Woodbury, Y. Liu, N. G. Walter, H. Yan, *Nat. Commun.* **2016**, *7*, 10619.
- [21] G. Ke, M. Liu, S. Jiang, X. Qi, Y. R. Yang, S. Wootten, F. Zhang, Z. Zhu, Y. Liu, C. J. Yang, H. Yan, *Angew. Chem., Int. Ed.* **2016**, *55*, 7483.
- [22] T. A. Ngo, E. Nakata, M. Saimura, T. Morii, *J. Am. Chem. Soc.* **2016**, *138*, 3012.
- [23] G. Grossi, M. Dalgaard Ebbesen Jepsen, J. Kjems, E. S. Andersen, *Nat. Commun.* **2017**, *8*, 992.
- [24] W. P. Klein, R. P. Thomsen, K. B. Turner, S. A. Walper, J. Vranish, J. Kjems, M. G. Ancona, I. L. Medintz, *ACS Nano* **2019**, *13*, 13677.
- [25] A. Rajendran, E. Nakata, S. Nakano, T. Morii, *ChemBioChem* **2017**, *18*, 696.
- [26] O. Idan, H. Hess, *ACS Nano* **2013**, *7*, 8658.
- [27] Y. Zhang, H. Hess, *ACS Catal.* **2017**, *7*, 6018.
- [28] C. Mukai, M. Bergkvist, J. L. Nelson, A. J. Travis, *Chem. Biol.* **2009**, *16*, 1013.
- [29] C. Mukai, L. Gao, M. Bergkvist, J. L. Nelson, M. M. Hinchman, A. J. Travis, *PLoS One* **2013**, *8*, e61434.
- [30] C. Mukai, L. Gao, J. L. Nelson, J. P. Lata, R. Cohen, L. Wu, M. M. Hinchman, M. Bergkvist, R. W. Sherwood, S. Zhang, A. J. Travis, *Angew. Chem., Int. Ed.* **2017**, *56*, 235.
- [31] A. Samanta, J. C. Breger, K. Susumu, E. Oh, S. A. Walper, N. Bassim, I. L. Medintz, *ACS Appl. Nano Mater.* **2018**, *1*, 3091.
- [32] S. A. Díaz, P. Choo, E. Oh, K. Susumu, W. P. Klein, S. A. Walper, D. A. Hastman, T. W. Odom, I. L. Medintz, *ACS Catal.* **2021**, *11*, 627.
- [33] K. Vogele, J. List, F. C. Simmel, T. Pirzer, *Langmuir* **2018**, *34*, 14780.
- [34] K. J. Koßmann, C. Ziegler, A. Angelin, R. Meyer, M. Skoupi, K. S. Rabe, C. M. Niemeyer, *ChemBioChem* **2016**, *17*, 1102.

- [35] S. Kröll, K. S. Rabe, C. M. Niemeyer, *Small* **2021**, *17*, 2105095.
- [36] B. Saccà, R. Meyer, M. Erkelenz, K. Kiko, A. Arndt, H. Schroeder, K. S. Rabe, C. M. Niemeyer, *Angew. Chem., Int. Ed.* **2010**, *49*, 9378.
- [37] R. Meyer, C. M. Niemeyer, *Small* **2011**, *7*, 3211.
- [38] M. Erkelenz, C.-H. Kuo, C. M. Niemeyer, *J. Am. Chem. Soc.* **2011**, *133*, 16111.
- [39] T. Burgahn, R. Garrecht, K. S. Rabe, C. M. Niemeyer, *Chem. Eur. J.* **2019**, *25*, 3483.
- [40] S. Kröll, L. Schneider, P. Wadhvani, K. S. Rabe, C. M. Niemeyer, *Chem. Commun.* **2022**, *58*, 13471.
- [41] E. Nakata, H. Dinh, T. A. Ngo, M. Saimura, T. Morii, *Chem. Commun.* **2015**, *51*, 1016.
- [42] M. Liu, J. Fu, X. Qi, S. Wooten, N. W. Woodbury, Y. Liu, H. Yan, *Chem-BioChem* **2016**, *17*, 1097.
- [43] T. M. Nguyen, E. Nakata, M. Saimura, H. Dinh, T. Morii, *J. Am. Chem. Soc.* **2017**, *139*, 8487.
- [44] M. Skoupi, C. Vaxelaire, C. Strohmann, M. Christmann, C. M. Niemeyer, *Chem. Eur. J.* **2015**, *21*, 8701.
- [45] Y. Hu, C. M. Domínguez, S. Christ, C. M. Niemeyer, *Angew. Chem., Int. Ed.* **2020**, *59*, 19016.
- [46] P. Bitterwolf, A. E. Zoheir, J. Hertel, S. Kröll, K. S. Rabe, C. M. Niemeyer, *Chem. Eur. J.* **2022**, *28*, e202202157.
- [47] N. H. Schlieben, K. Niefind, J. Müller, B. Riebel, W. Hummel, D. Schomburg, *J. Mol. Biol.* **2005**, *349*, 801.
- [48] C. E. Quartararo, S. Hazra, T. Hadi, J. S. Blanchard, *Biochemistry* **2013**, *52*, 1765.
- [49] A. Cornish-Bowden, *Fundamentals of Enzyme Kinetics*, 4th ed., Wiley, Weinheim, Germany **2012**.
- [50] T. Peschke, M. Skoupi, T. Burgahn, S. Gallus, I. Ahmed, K. S. Rabe, C. M. Niemeyer, *ACS Catal.* **2017**, *7*, 7866.
- [51] P. Bitterwolf, S. Gallus, T. Peschke, E. Mittmann, C. Oelschlaeger, N. Willenbacher, K. S. Rabe, C. M. Niemeyer, *Chem. Sci.* **2019**, *10*, 9752.
- [52] L. Meng, Y. Liu, X. Yin, H. Zhou, J. Wu, M. Wu, L. Yang, *Appl. Biochem. Biotechnol.* **2020**, *190*, 880.
- [53] M. Dias Gomes, J. M. Woodley, *Molecules* **2019**, *24*, 3573.
- [54] H. Jörnvall, B. Persson, M. Krook, S. Atrian, R. Gonzalez-Duarte, J. Jeffery, D. Ghosh, *Biochemistry* **1995**, *34*, 6003.
- [55] V. Linko, M. Eerikäinen, M. A. Kostianen, *Chem. Commun.* **2015**, *51*, 5351.
- [56] R. Kosinski, J. M. Perez, E.-C. Schöneweiß, Y. B. Ruiz-Blanco, I. Ponzio, K. Bravo-Rodriguez, M. Erkelenz, S. Schlücker, G. Uhlenbrock, E. Sanchez-Garcia, B. Saccà, *Sci. Adv.* **2022**, *8*, eabk0425.
- [57] Y. Zhang, S. Tsitkov, H. Hess, *Nat. Commun.* **2016**, *7*, 13982.
- [58] P. Lin, H. Dinh, Y. Morita, Z. Zhang, E. Nakata, M. Kinoshita, T. Morii, *Chem. Commun.* **2021**, *57*, 3925.
- [59] S. K. Pal, L. Zhao, A. H. Zewail, *Proc. Natl. Acad. Sci. U. S. A.* **2003**, *100*, 8113.
- [60] Y. Xiong, S. Tsitkov, H. Hess, O. Gang, Y. Zhang, *ACS Nano* **2022**, *16*, 10383.
- [61] W. Abdallah, V. Chirino, I. Wheeldon, S. Banta, *ChemBioChem* **2019**, *20*, 1827.
- [62] J. N. Vranish, M. G. Ancona, E. Oh, K. Susumu, G. Lasarte Aragonés, J. C. Breger, S. A. Walper, I. L. Medintz, *ACS Nano* **2018**, *12*, 7911.
- [63] M. Arrio-Dupont, P. R. Coulet, D. C. Gautheron, *Biochim. Biophys. Acta* **1985**, *829*, 58.
- [64] F. Jia, B. Narasimhan, S. K. Mallapragada, *AIChE J.* **2013**, *59*, 355.
- [65] Y. Zhang, Y. Yong, J. Ge, Z. Liu, *ACS Catal.* **2016**, *6*, 3789.
- [66] P. Lin, H. Dinh, E. Nakata, T. Morii, *Chem. Commun.* **2021**, *57*, 11197.
- [67] J. C. Breger, J. N. Vranish, E. Oh, M. H. Stewart, K. Susumu, G. Lasarte-Aragonés, G. A. Ellis, S. A. Walper, S. A. Díaz, S. L. Hooe, W. P. Klein, M. Thakur, M. G. Ancona, I. L. Medintz, *Nat. Commun.* **2023**, *14*, 1757.
- [68] L. Schneider, K. S. Rabe, C. M. Domínguez, C. M. Niemeyer, *ACS Nano* **2023**, *17*, 6719.
- [69] Z. Wang, E. St. Iago-Mcrae, A. Ebrahimiojarad, S. Won Oh, J. Fu, *Langmuir* **2022**, *38*, 12594.
- [70] X. Li, X. Cao, J. Xiong, J. Ge, *Small* **2020**, *16*, 1902751.
- [71] H. Xia, N. Li, W. Huang, Y. Song, Y. Jiang, *ACS Appl. Mater. Interfaces* **2021**, *13*, 22240.
- [72] R. Greifenstein, T. Ballweg, T. Hashem, E. Gottwald, D. Achauer, F. Kirschhöfer, M. Nusser, G. Brenner-Weiß, E. Sedghamiz, W. Wenzel, E. Mittmann, K. S. Rabe, C. M. Niemeyer, M. Franzreb, C. Wöll, *Angew. Chem., Int. Ed.* **2022**, *61*, e202117144.
- [73] W. Liang, P. Wied, F. Carraro, C. J. Sumbly, B. Nidetzky, C.-K. Tsung, P. Falcaro, C. J. Doonan, *Chem. Rev.* **2021**, *121*, 1077.
- [74] J. S. Hertel, P. Bitterwolf, S. Kröll, A. Winterhalter, A. J. Weber, M. Grösche, L. B. Walkowsky, S. Heißler, M. Schwotzer, C. Wöll, T. Van De Kamp, M. Zuber, T. Baumbach, K. S. Rabe, C. M. Niemeyer, *Adv. Mater.* **2023**, *2303952*.